Measurement Science and Technology

100 year anniversary
Measurement Science and Technology

PAPER

Multisource cross-domain fault diagnosis of rolling bearing based on subdomain adaptation network

To cite this article: Zhichao Wang *et al* 2022 *Meas. Sci. Technol.* **33** 105109

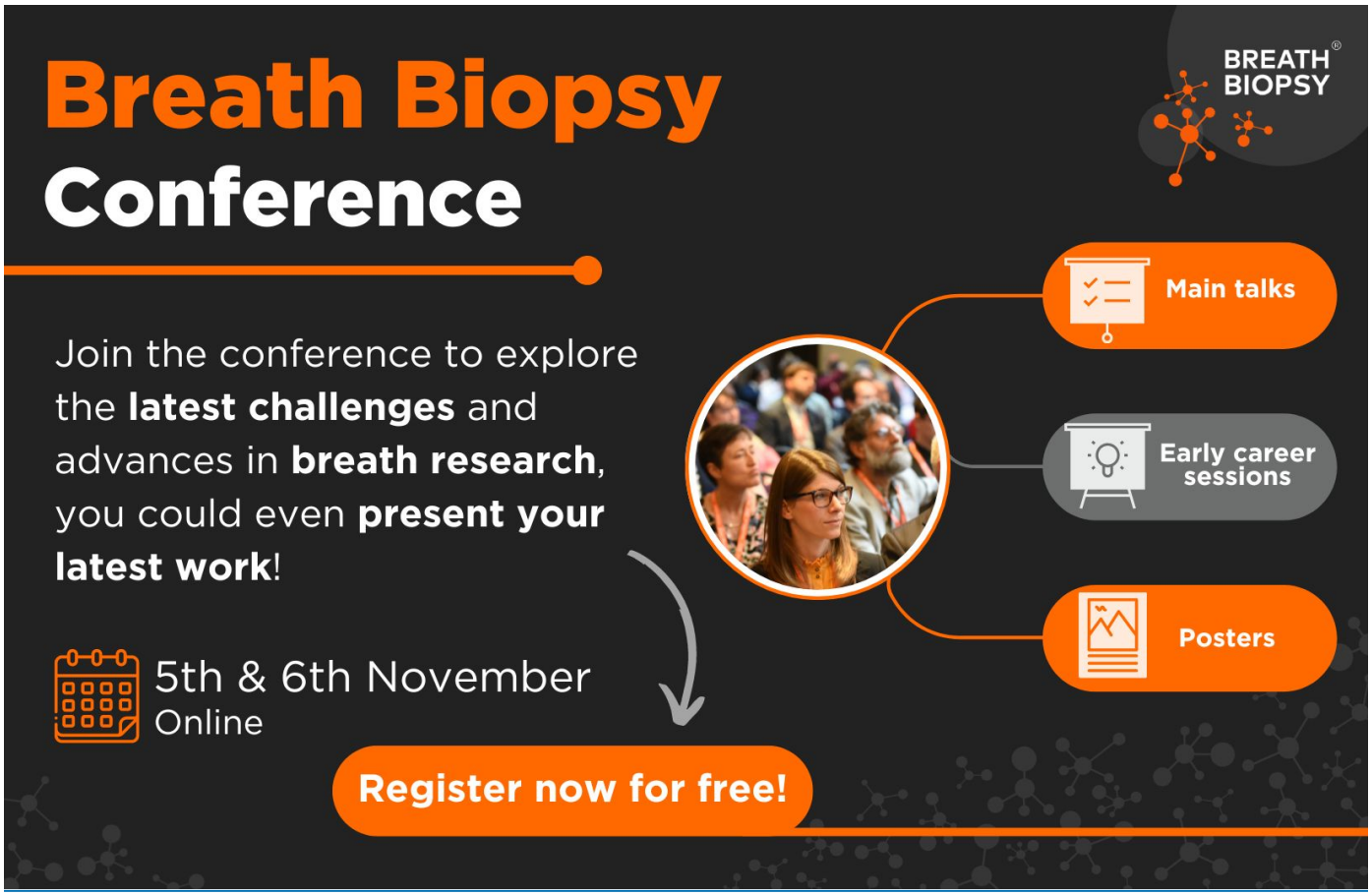

IOP Publishing Measurement Science and Technology
Meas. Sci. Technol. **33** (2022) 105109 (15pp) https://doi.org/10.1088/1361-6501/ac7941

Multisource cross-domain fault diagnosis of rolling bearing based on subdomain adaptation network

Zhichao Wang, Wentao Huang*, Yi Chen, Yunchuan Jiang and Gaoliang Peng

School of Mechatronics Engineering, Harbin Institute of Technology, 92 West Dazhi Street, Harbin, People's Republic of China

E-mail: hwt@hit.edu.cn

Received 3 March 2022, revised 3 June 2022
Accepted for publication 15 June 2022
Published 14 July 2022

Abstract

The excellent performance of current intelligent fault diagnosis methods based on deep learning is attributed to the availability of large amounts of labeled data. However, in practical bearing fault diagnosis, the high cost of large sample data and changes in operating conditions lead to the scarcity of available training data, which limits the engineering application of intelligent bearing fault diagnosis. To solve this problem, this paper proposes a cross-domain fault diagnosis method based on multisource subdomain adaptation networks (MSDAN). First, the data from multiple source domains are simultaneously input to a shared feature extractor composed of a one-dimensional residual network. Then, the private feature extractor is used to learn features from different source domains and reduce the domain shifts of each source and target domain using the local maximum mean discrepancy. Finally, the different classifier outputs of the target domain samples are aligned. The highlight of MSDAN is to obtain diagnostic knowledge from multiple source domains and further divide the subdomains using the categories as criteria, which not only aligns the global distribution of the source and target domain but also performs a more refined subdomain alignment. The method effectively alleviates the negative transfer phenomenon caused by insufficient domain alignment in multisource transfer diagnosis. The effectiveness and superiority of the proposed MSDAN method are verified by constructing seven multisource transfer tasks with two bearing fault diagnosis cases, including cross-operating-condition and cross-machine.

Supplementary material for this article is available online

Keywords: intelligent fault diagnosis, transfer learning, multisource, subdomain adaptation, rolling bearing

(Some figures may appear in colour only in the online journal)

1. Introduction

In actual industry, the health condition of rolling bearings is a key factor in the normal operation of mechanical equipment, so the fault diagnosis of rolling bearing health conditions is particularly important [1]. Traditional fault diagnosis methods are usually divided into four steps: signal processing, feature extraction, feature selection and fault classification [2]. The diagnosis of the health condition of rolling bearings is obtained through the expertise of engineers. However, if the manually selected features are of poor quality, the performance of fault classification is greatly reduced and the above techniques need to be tailored to different machines and operating conditions,

* Author to whom any correspondence should be addressed.

which does not meet the needs of automated diagnosis in industrial scenarios [3]. In recent years, fault diagnosis has gradually shifted from traditional diagnostic algorithms to deep feature mining methods for highly non-linear, complex and multi-dimensional systems [4]. In particular, with the rapid development of deep learning technology [5], the diagnostic framework based on deep learning has shown good performance in learning advanced features [6], providing a powerful solution to overcome the above-mentioned obstacles in rolling bearing fault diagnosis, which has achieved certain results [7–10].

However, intelligent diagnostic methods based on deep learning do not work well in practical applications [11]. On the one hand, mechanical equipment is usually in a healthy state during actual operation and accessible fault samples are severely scarce [12]. On the other hand, the above models also have limitations when dealing with changing operating conditions [13]. To this end, domain adaptation [14] is introduced to the cross-domain bearing fault diagnosis task to address the two problems mentioned above [15]. As a type of transfer learning, domain adaptation adapts the data distribution between the source domain data with labeled fault categories and the target domain data with incomplete or unlabeled fault categories by extracting domain-invariant features [16] between the two datasets in order to reduce data distribution differences and improve the diagnostic performance of the target domain. The existing domain adaptation techniques for fault diagnosis consist of two main types. The first type is the adaptation network based on statistical moment matching of features [17], which maps the transferable features into the reproducing kernel Hilbert space (RKHS) to reduce the distribution discrepancy between the source and target domain by minimizing non-parametric metric distances [18–21], such as maximum mean discrepancy (MMD) [22], multi-kernel maximum mean discrepancies (MK-MMDs) [23], Wasserstein distance [24], etc. The second type of adaptation network is based on adversarial learning [25], which has a feature generator and a domain discriminator. The domain discriminator will not discriminate between the source and target domain by training the network structure, thus allowing the model to handle both domains well [26–29].

The above research on domain adaptation techniques has effectively improved improving the performance of cross-domain fault diagnosis. Nevertheless, the above studies are limited to single-source domain adaptation. In practical applications, more than one source domain may be used for training [30]. If only one source domain is used for training, it is obviously wasteful. Consequently, making full use of multiple source domains for domain adaptation can provide a broader and more comprehensive diagnostic knowledge [31]. Currently, multisource domain adaptation has been applied in the field of fault diagnosis. For example, Zheng *et al* [32] mapped different source domain data into the Grassmann manifolds and then derived the average subspace of all source domains by Karcher averaging to adapt the distribution of the target domain. Zhang *et al* [33] organically combined multi-source domain data by gradient inversion layer to achieve the confusion of multi-domain features and reduce the prediction inconsistency of multi-classifiers. Wei *et al* [34] proposed a weighted domain adaptation network. In this study, different source domains were assigned corresponding weights by measuring the MMD loss between each source domain and the target domain and a domain adaptation threshold was set to prevent the negative transfer, which improves the effectiveness of multisource domain adaptation. Yang *et al* [35] utilized stack sparse auto-encoder (SSAE) and K-means to extract better domain-invariant and discriminative features from multi-source domain data, and finally obtained a fault diagnosis model that is better than single-source domain transfer.

Although existing studies have achieved good results in the area of multisource domain fault diagnosis, they have mainly focused on learning a generic invariant representation of all domains. The global distribution of source domains and the target domain is adaptively aligned without considering domain-specific decision boundaries between categories [36]. Therefore, there is no guarantee that samples from different domains but from the same category will be precisely mapped together in the feature space after global alignment, resulting in poor fault diagnosis rates for the target domain. Furthermore, differences between a single source domain and a target domain cannot be precisely eliminated. When attempts are made to align multiple source domains and the target domain, even greater errors may arise. In contrast, subdomain adaptation divides the domain into subdomains using categories as criteria. After subdomain adaptation, the local distribution is similar, so the global distribution is more similar. Based on these considerations, we believe it is important to investigate the differences in subdomain distribution between multiple source domains and the target domain in fault diagnosis applications.

In this paper, we propose a multisource domain adaptation network based on subdomain feature alignment, which aims to improve the diagnostic accuracy of the unlabeled target domain. Our motivations are (a) collecting data from multiple source domains to match a common target domain, providing a broader diagnostic knowledge for the training process and (b) more refined subdomain alignment is used to attenuate the effects of negative transfer. Specifically, a shared feature extractor consisting of a one-dimensional residual network is designed to learn generic features, while multiple source domains and the target domain data from different distributions are mapped to multiple different feature spaces using a private feature extractor. Furthermore, local maximum mean discrepancy (LMMD) constraints are introduced to capture the multimodal underlying features of the data distribution, which are precisely aligned for the same fault category. In addition, using domain-specific decision boundaries, the output of the classifier can be aligned to the target sample.

The main contributions of this paper are summarized as follows.

(a) The collected raw vibration signals are directly used as the input to the network, which avoids the tedious data preprocessing and time-frequency conversion process, thus realizing the end-to-end fault diagnosis.

(b) An unsupervised intelligent fault diagnosis method is proposed, which considers a more comprehensive domain feature alignment. Accordingly, not only the whole feature space is aligned but also the space of each subclass.
(c) It is an unsupervised multisource domain adaptation method for the case where the target domain is unlabeled, which can be applied to fault diagnosis across operating conditions and across machines.

2. Related works

2.1. Problem formulation

The task of multisource domain adaptation for rolling bearing fault diagnosis is to combine multiple sets of labeled source domain data and unlabeled target domain data to minimize the classification error of the data to be diagnosed. The difficulty lies in the fact that the data distribution of the source domains and the target domain is different, and the distribution of different source domains is also different. In unsupervised multisource domain adaptation, we are given N datasets with labels under different operating conditions or machines as N source domains.

Let $\mathcal{D}_{s(j)} = \{x_i^s, y_i^s\}_{i=1}^{n_s} (i = 1, 2, \ldots, n_s, j = 1, 2, \ldots, N)$ be the source domain j, where $X_{s(j)} = \left\{x_i^{s(j)}\right\}_{i=1}^{n_s}$ denotes the labeled data sample from source domain j, and the corresponding health status is denoted as $Y_{s(j)} = \left\{y_i^{s(j)}\right\}_{i=1}^{n_s}$. In addition, the unlabeled data to be diagnosed is used as the target domain, denoted as $\mathcal{D}_t = \{x_i^t, y_i^t\}_{i=1}^{n_t} (i = 1, 2, \ldots, n_s)$, where $X_t = \{x_i^t\}_{i=1}^{n_t}$ indicates the target domain data. Significantly, the target label $Y_t = \{y_i^t\}_{i=1}^{n_t}$ cannot be used for training, but only for testing. In this study, the following two main assumptions are followed.

(a) The health condition space is the same under all operating conditions or machines, i.e. the source domains and the target domain have the same label space.
(b) The data under all conditions or machines share the same feature space, i.e. the data distribution between the source domains and the target domain is different but similar.

2.2. Multisource subdomain adaptation (MSSA)

Previous fault diagnosis methods based on multisource domain adaptation have focused on aligning the global distribution between different domains, which can lead to misclassification of data that are too close to each other at decision boundaries. As shown in figure 1, we can use the correlation between samples to subdivide the domain further into subdomains by using the category as a criterion. For the source domain, we can use the true labels of the source samples to divide it into multiple subdomains. In contrast, the labels of the target domain are unknown during the training process, and typically we can use the predicted probability output of the network model as a pseudo-label to subdivide the target domain [37]. Based on this partitioning criterion, the distribution of the relevant subdomains of samples with the same label is aligned so that the whole domain is further aligned by local subdomain alignment, which is obviously a more fine-grained alignment than global domain adaptation and is conducive to improving fault diagnosis accuracy.

2.3. Local maximum mean discrepancy (LMMD)

In previous cross-domain fault diagnosis tasks, it has been an effective method to measure the similarity of feature distribution from different domains based on the MMD criterion. We assume that the source domain $\mathcal{D}_s$ and target domain $\mathcal{D}_t$ follow probability distribution p and q, respectively. The mathematical expression for the MMD between $\mathcal{D}_s$ and $\mathcal{D}_t$ is formulated as:

$$\mathrm{MMD}^2(D_s, D_t) \triangleq \|E_p[\phi(x^s)] - E_q[\phi(x^t)]\|_{\mathcal{H}}^2 \tag{1}$$

where $\mathcal{H}$ represents the RKHS, $\phi(\cdot)$ indicates a non-linear mapping from the original feature space to the RKHS [38].

However, MMD is an alignment of global domain feature distribution, which ignores the relationship of subdomains between the source domain and target domain. Considering the correlation between samples of the same category, LMMD is introduced in this paper for aligning the distribution between the relevant subdomains of the same category. Accordingly, $\mathcal{D}_s$ and $\mathcal{D}_t$ can be divided into K subdomains, where K is the number of fault categories. The mathematical expression for the LMMD between $\mathcal{D}_s$ and $\mathcal{D}_t$ can be expressed as follows:

$$\mathrm{LMMD}^2(\mathcal{D}_s, \mathcal{D}_t) \triangleq E_c \left\|E_{p(k)}[\phi(x^s)] - E_{q(k)}[\phi(x^t)]\right\|_{\mathcal{H}}^2 \tag{2}$$

where x^s and x^t are the instances of $\mathcal{D}_s$ and $\mathcal{D}_t$, respectively, $p(k)$ and $q(k)$ are the distributions of subdomain $\mathcal{D}_s^{(k)}$ and $\mathcal{D}_t^{(k)}$, respectively. In contrast to the global distribution differences calculated by MMD, the above formula calculates the local distribution differences. By minimizing the distribution of the relevant subdomains, the domain distributions of the same categories will be aligned closer together. In order to express LMMD more clearly, we introduce the concept of sample weights. Thus, the unbiased estimate of LMMD can be defined as:

$$\mathrm{LMMD}^2(\mathcal{D}_s, \mathcal{D}_t) = \frac{1}{K}\sum_{k=1}^{K}\left\|\sum_{x_i^s \in \mathcal{D}_s} \omega_i^{sk}\phi(x_i^s) - \sum_{x_j^t \in \mathcal{D}_t} \omega_j^{tk}\phi(x_j^t)\right\|_{\mathcal{H}}^2 \tag{3}$$

where ω_i^{sk} and ω_i^{tk} represent the weights of the source domain sample x_i^s and the target domain sample x_j^t belonging to category k, respectively. For the sample x^i, its weight ω_k^i can be represented as:

$$\omega_i^k = \frac{y_{ik}}{\sum_{(x_j, y_j) \in \mathcal{D}} y_{jk}} \tag{4}$$

where y_{ik} is the kth element of the label vector y_i, representing the probability of the sample belonging to category k. $\sum_{(x_j, y_j) \in \mathcal{D}} y_{jk}$ is the sum of the probabilities of all samples in the domain $\mathcal{D}$ belonging to category k. When the domain $\mathcal{D}$

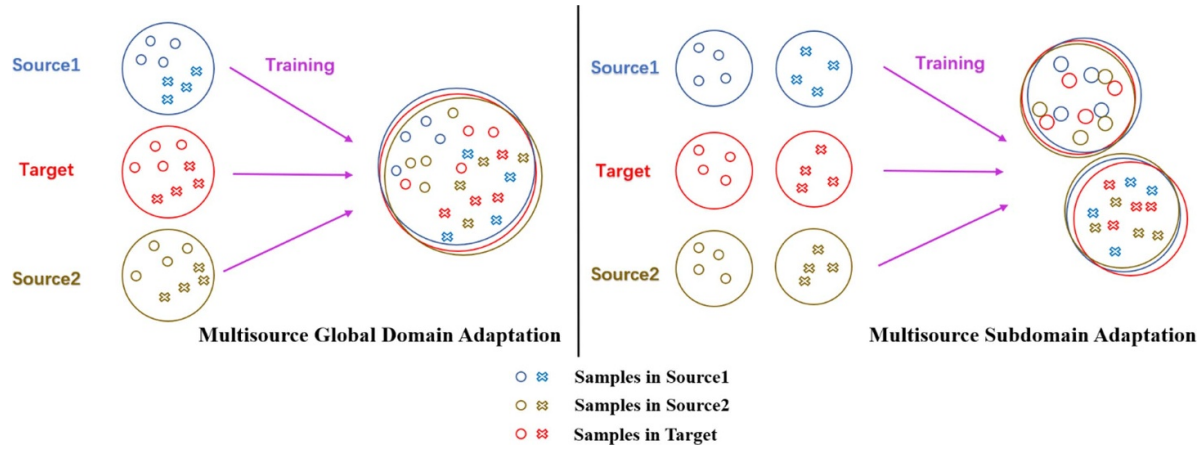

Figure 1. Multisource global domain adaptation and multisource subdomain adaptation (MSSA).

represents the source domain, we can use the true label y_s^i of the sample x_s^i in the source domain to calculate the weight ω_i^{sk} of the samples belonging to category k. Although there is no available labeled data in the target domain, it is feasible to use the softmax output $\hat{y}_i^t$ of the classifier to calculate the weight ω_i^{tk} of the sample x_i^t in the target domain belonging to category k.

The RKHS $\mathcal{H}$ has the inner product completeness property $< \phi(x^s), \phi(x^t) >= \mathcal{K}(x^s, x^t)$ where $< \cdot, \cdot >$ denotes the inner product of vectors and $\mathcal{K}$ denotes the kernel function, thus the samples can be mapped into higher order moments by kernel embedding. Assuming that the output of the samples in the source domain and the target domain after the feature extraction of the network layer L is z_i^{sl} and z_i^{tl}, the calculation of the distance between the source domain distribution and the target domain distribution can be converted to the kernel function form:

$$\begin{aligned}\mathrm{LMMD}^2(\mathcal{D}_s, \mathcal{D}_t) = \frac{1}{K}\sum_{k=1}^{K}\Bigg[&\sum_{i=1}^{n_s}\sum_{j=1}^{n_s}\omega_i^{sk}\omega_j^{sk}\mathcal{K}\left(z_i^{sl}, z_j^{sl}\right) \\ &+\sum_{i=1}^{n_t}\sum_{j=1}^{n_t}\omega_i^{tk}\omega_j^{tk}\mathcal{K}\left(z_i^{tl}, z_j^{tl}\right) \\ &-2\sum_{i=1}^{n_x}\sum_{j=1}^{n_t}\omega_i^{sk}\omega_j^{tk}\mathcal{K}\left(z_i^{sl}, z_j^{tl}\right)\Bigg]\end{aligned} \tag{5}$$

3. The proposed method

In this section, we propose a multisource domain adaptation network framework based on subdomain feature alignment as shown in figure 2. It can be seen that this framework includes a shared feature extractor, multiple private feature extractors and multiple classifiers. In the first stage, the framework maps each pair of data from the source domain and the target domain to a specific feature space and matches the distribution between them utilizing LMMD constraints. In the second stage, the target sample outputs of multiple domain-specific classifiers are aligned by mean differences. In this diagnostic process, the ultimate optimization goal of the proposed multisource subdomain adaptation (MSSA) network (MSDAN) is to learn category-identification and domain invariant representation as well as to minimize the differences between classifiers.

In the following part of this section, section 3.1 presents the architecture of the proposed MSDAN, and section 3.2 describes the optimization goals of MSDAN. The training procedure of MSDAN will be explained in section 3.3.

3.1. MSDAN architecture

Considering that modern intelligent fault diagnosis requires little expert experience on signal processing, the raw vibration signals, including the N source domain datasets and a target domain dataset, are directly fed into a shared feature extractor. All domains share a shared feature extractor for certain generic shallow features to be learned. We propose a common subnet $f(^*)$ to extract common representations of all domains that map the signal from the original feature space to the common feature space. In order to extract features efficiently, a one-dimensional residual network is designed as the shared feature extractor for processing the original vibration signal. The structure parameters of this 1D residual network are shown in figure 3, which mainly consists of a convolutional pooling module and four residual blocks. In this paper, we use a residual block containing two convolutional layers with a convolutional kernel size of 3×1, both with an output channel number of 20 and a step size of 1, and all the convolutional layers adopt a zero-padding strategy. In addition, in order to facilitate back propagation of errors, each convolution in the residual block is followed by a batch normalization and then activated using the rectified linear unit (ReLU) function.

For multiple source domains, it is difficult to learn a generic domain invariant representation. Therefore, we hope that data from different source domains have their own private feature extractors and that the common features are mapped into a private feature space. In our network, there are N subnets which are specific to the source domain. Each subnet

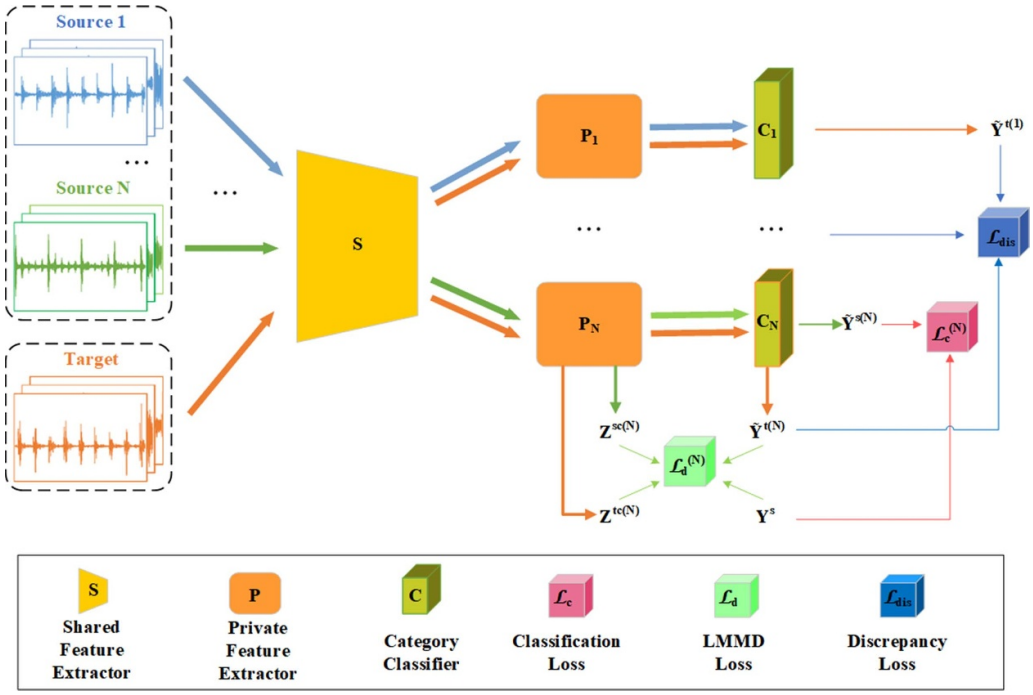

Figure 2. Overall framework of the proposed MSDAN.

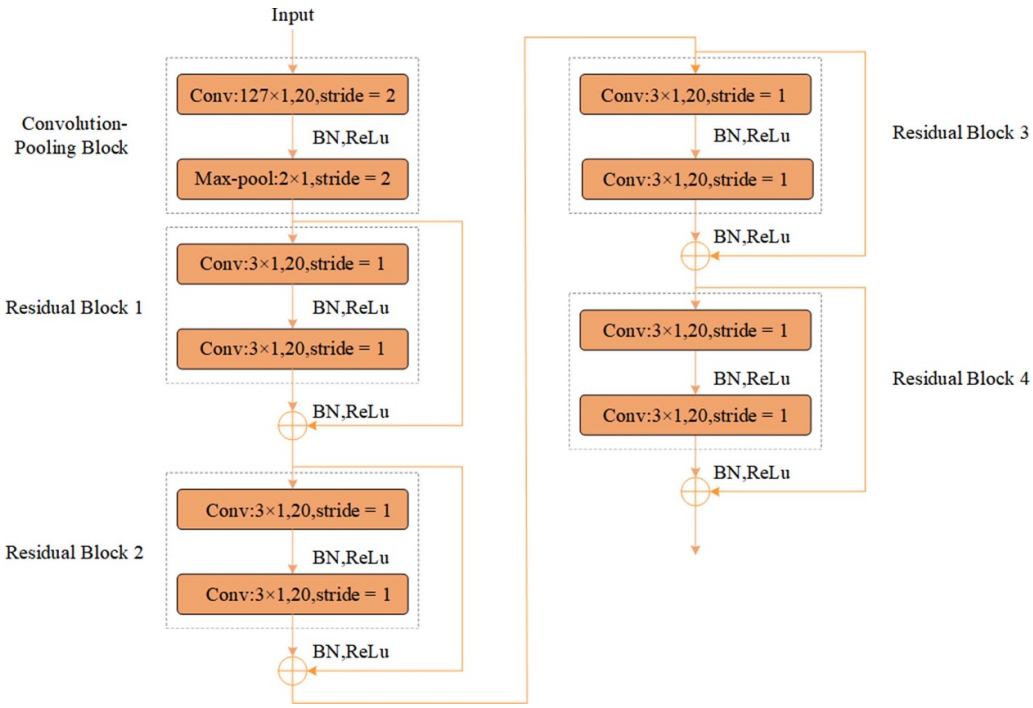

Figure 3. Network structure of the shared feature extractor.

contains two convolutional layers with a convolutional kernel of 3 × 1 and an average-pooling layer. For the subnets of different domains, no weights are shared between them. The domain-specific private feature extractor feeds the extracted common features into a specific non-shared domain subnet $h_j(^*)$ depending on the source domain, and maps each pair of source domain and target domain to a specific feature space. Subsequently, the network will learn a domain-specific classifier for each non-shared subnet.

3.2. Optimization objective

In this subsection, the optimization objective of MSDAN is introduced in detail. As shown in figure 2, the optimization

Algorithm 1. Training procedure of MSDAN.

Input: Labeled source domain datasets $\left\{\mathcal{D}_j^s\right\}_{j=1}^N = \left\{\left\{x_i^{sj}, y_i^{sj}\right\}_{i=1}^{n_s}\right\}_{j=1}^N$; Unlabeled target domain datasets $\mathcal{D}^t = \{x_i^t\}_{i=1}^{n_t}$; Batch size b; The number of training iterations; Shared feature extractors S; Private feature extractors $\{P_j\}_{j=1}^N$; Category classifiers $\{C_j\}_{j=1}^N$.
Output: Diagnostic results $\{y_i^t\}_{i=1}^{n_t}$.
1: **for** iterations = 1 **to** iterations **do**:
2: **for** j = 1 **to** N **do**:
3: Randomly samples $S_j = \{x_i^{sj}, y_i^{sj}\}_{i=1}^b$, $\mathcal{T} = \left\{x_i^{tj}\right\}_{i=1}^b$ from $\mathcal{D}_j^s$ and $\mathcal{D}^t$ respectively;
4: Forward propagation of MSDAN.
(a) calculate the output of the shared extractor and N private extractors of source domain samples and target domain samples. $Z_i^{sj} \leftarrow P_j(S(x_i^s))$, $\{Z_i^{tm}\}_{m=1}^N \leftarrow \{P_m(S(x_i^t))\}_{m=1}^N$
(b) calculate the output of the jth category classifier of source domain samples. $\hat{y}_i^s = C_j(Z_i^j)$
(c) calculate the output of category classifiers of target domain samples.$\{\hat{y}_i^{tm}\}_{m=1}^N = \{C_m(Z_i^{tm})\}_{m=1}^N$
(d) calculate the total optimization objective by equations (6)–(8). $\mathcal{L} = \mathcal{L}_{cls} + \alpha\mathcal{L}_{lmmd} + \beta\mathcal{L}_{dis}$
5: Backward update $\theta_s, \theta_p^j|_{j=1}^N, \theta_c^j|_{j=1}^N$.
6: **end for**
7: **end for**

objective of MSDAN consists of three main components. The first part aims to minimize the domain-specific loss function of the classifier on the source domain dataset. The classifier C_j is a softmax classifier specific to the source domain $\mathcal{D}_{s(j)}$. By iteratively training the shared feature extractor S, the private feature extractor P_j and the classifier C_j, we can obtain more task discriminative features. The loss function of the classifier can be expressed as:

$$\begin{aligned}\mathcal{L}_{\text{cls}} &= \sum_{j=1}^{N} \mathcal{L}_{\text{cls}}^j(C_j(P_j(S(x_i^{sj}))), y_i^{sj}) \\ &= \sum_{j=1}^{N}\left[\frac{1}{n_s}\sum_{i=1}^{n_s} J_y(C_j(P_j(S(x_i^{sj}))), y_i^{sj})\right]\end{aligned} \tag{6}$$

where $J_y(\cdot,\cdot)$ stands for the cross-entropy loss function.

In contrast to previous approaches to global alignment of domain adaptation, MSDAN considers the relationship between subdomains and aligns the feature distribution between the source domain and target domain more finely. Hence, the second optimization objective of MDSAN is the difference between the subdomain distribution. We use equation (5) to calculate the local maximum mean discrepancy (LMMD) loss between each pair of source domain and target domain, which is described as follows:

$$\mathcal{L}_{\text{lmmd}} = \frac{1}{N}\sum_{j=1}^{N} \text{LMMD}^2(\mathcal{D}_{s(j)}, \mathcal{D}_t). \tag{7}$$

In multisource domain adaptation, different source domains may have different transitivity relative to the target domain, which will lead to differences in the predictions of classifiers from different source domains for the target samples (especially those near the category boundary). Therefore, the third optimization goal of MDSAN is to minimize the differences between multiple classifiers. Using the idea of mean differences, the loss function is calculated as follows:

$$\begin{aligned}\mathcal{L}_{\text{dis}} = \frac{1}{N\times(N-1)}\sum_{j=1}^{N-1}\sum_{i=j+1}^{N}\mathbb{E}_{x\sim X_t} \\ \times\left[\left|C_j(P_j(S(x_k^t))) - C_i(P_j(S(x_k^t)))\right|\right].\end{aligned} \tag{8}$$

Therefore, the final total loss function can be written as:

$$\mathcal{L} = \mathcal{L}_{\text{cls}} + \alpha\mathcal{L}_{\text{lmmd}} + \beta\mathcal{L}_{\text{dis}} \tag{9}$$

where $\alpha > 0$ and $\beta > 0$ stand for tradeoff parameters that control the interaction of the loss terms. In the training process of our model, in order to speed up the gradient descent, we used the stochastic gradient descent (SGD) algorithm for optimizing equation (9). Let $\Theta = \{\theta_s, \{\theta_p^j\}_{j=1}^N, \{\theta_c^j\}_{j=1}^N\}$ denote the parameters of the shared feature extractor, private feature extractors and category classifier, respectively. The optimization of the total loss function is to find the optimum values of θ_s^*, $\{\theta_p^{j*}\}_{j=1}^N$ and $\{\theta_c^{j*}\}_{j=1}^N$. Therefore, equation (9) can be redefined as:

$$\begin{aligned}&\mathcal{L}\left(\theta_s^*, \theta_p^{j*}|_{j=1}^N, \theta_c^{j*}|_{j=1}^N\right) \\ &= \min_{\theta_s, \theta_p^j|_{j=1}^N, \theta_c^j|_{j=1}^N}\left(\begin{array}{l}\mathcal{L}_{\text{cls}}\left(\theta_s, \theta_p^j|_{j=1}^N, \theta_c^j|_{j=1}^N\right) \\ \quad +\alpha\mathcal{L}_{\text{lmmd}}\left(\theta_s, \theta_p^j|_{j=1}^N, \theta_c^j|_{j=1}^N\right) \\ \quad +\beta\mathcal{L}_{\text{dis}}\left(\theta_s, \theta_p^j|_{j=1}^N, \theta_c^j|_{j=1}^N\right)\end{array}\right).\end{aligned} \tag{10}$$

3.3. Training procedure

The pseudo code of our proposed MSDAN training procedure is summarized in algorithm 1. Based on equation (10) and the SGD optimization algorithm, the parameter set can be continuously updated until an intelligent diagnostic model that can accurately classify the unlabeled target domain data is obtained.

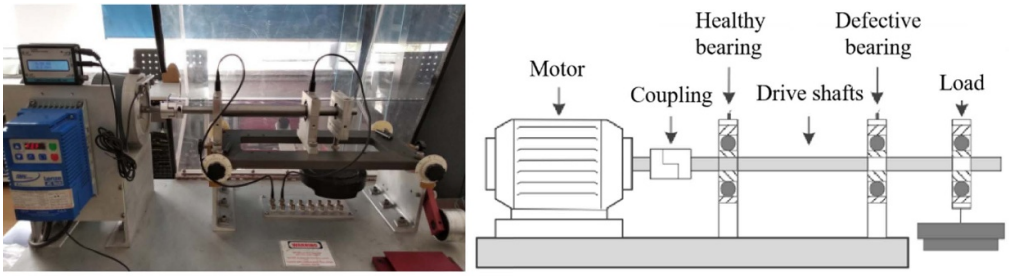

Figure 4. Comprehensive simulation test rig for mechanical fault: (a) photo of the test rig and (b) schematic diagram of the test rig.

4. Experiment

In this section, we conduct extensive experiments on two bearing fault diagnosis cases to verify the effectiveness of the MSDAN method. The computational experiments are based on the Pycharm integrated environment to complete the debugging of the code, using Pytorch 1.4.0 + CUDA 10.1 as the deep learning development framework. To speed up training, all experimental methods were run on a GTX1650 graphics card.

4.1. Case I: fault diagnosis on variable operating condition

4.1.1. Dataset description. The experimental data for this case was collected through the 'Machinery Fault Simulator' (MFS), a mechanical fault comprehensive simulation test rig developed by SpectraQuest. The specific construction of the test rig is illustrated in figure 4. The test rig has a 1 hp motor with a maximum speed of 100 Hz and can be fitted with two bearings at the same time for data acquisition purposes. The bearing vibration signals can be acquired using an SQI608A11-3F/8 accelerometer with a maximum sampling frequency of 102.4 kHz, while the rotor on the shaft can provide radial loads for both bearings. In this case, the bearings were cantilevered with a load of 5 kg, and the vibration signals were acquired at a sampling frequency of 51.2 kHz.

In order to verify the validity of the proposed method, a simulation of a single point fault was carried out on the inner and outer raceway surfaces of 6205 deep groove ball bearings by electrical discharge machining (EDM). It is worth noting that the magnitude of the bearing failures involved in this paper is expressed in terms of the size of the circular center angle and the depth of the defect in the circular part of the bearing raceway occupied by the failed area. As shown in figure 5, there are six categories of bearing faults: slight fault of inner raceway ($\varphi_d = 2°$, $h_{\max} = 0.1$ mm), moderate fault of inner raceway ($\varphi_d = 5°$, $h_{\max} = 0.1$ mm), severe fault of inner raceway ($\varphi_d = 8°$, $h_{\max} = 0.1$ mm), slight fault of outer raceway ($\varphi_d = 2°$, $h_{\max} = 0.1$ mm), moderate fault of outer raceway ($\varphi_d = 5°$, $h_{\max} = 0.1$ mm) and severe fault of outer raceway ($\varphi_d = 8°$, $h_{\max} = 0.1$ mm). The widths of the faults were machined to 2.26 mm.

In the experiment, we randomly intercepted 8192 data points from the original vibration signal as a sample, and each health condition contains 500 samples. Meanwhile, three datasets were created according to different drive speeds: 600 rpm (R_1), 900 rmp (R_2) and 1200 rmp (R_3), where each dataset includes seven categories of health conditions, i.e. N, IR2, IR5, IR8, OR2, OR5, OR8. The details description is presented in table 1. Based on the multisource domain adaptation scenario, we treated each dataset as a domain and created the three multisource domain adaptation tasks in table 2. It is noted that the source domain samples used for training and the target domain samples used for testing are labeled, while the target domain samples for training are unlabeled.

4.1.2. Comparison approaches and training details. In order to comprehensively validate the effectiveness and superiority of the proposed method (MSDAN), eight popular intelligent fault diagnosis methods which have similar network structure and experimental settings with the MSDAN are selected for comparison, including single-source domain and multisource domain adaptation methods. The application details are described as follows.

(a) Single-best DA: This part applies single-source domain adaptation methods to perform domain adaptation on each source domain and target domain, respectively, and selects the result with the best target domain recognition as the experimental result. Four classical deep transfer learning methods are selected, including Baseline, Deep Domain Confusion (DDC) [39], Deep Adaptation Networks (DAN) [40], and Domain-Adversarial Neural Networks (DAAN) [41]. Baseline is a basic convolutional network but without domain adaptation, in which only the source domain is used for training, and the target domain is used for testing. DDC completes the adaptive adjustment of the source domain and target domain by adding an adaptive layer to the Baseline network to measure the MMD loss between the two domains. DAN adds the MK-MMD loss based distributional adaptation module to our Resnet network. DANN is a domain adaptation method based on adversarial networks.

(b) Source-combine DA: It is an approach that combines multiple source domains into a single source domain, using a single source domain approach to solve the problem of multiple source domains, including DAN adaptation method based on feature alignment and DAAN adaptation method based on adversarial.

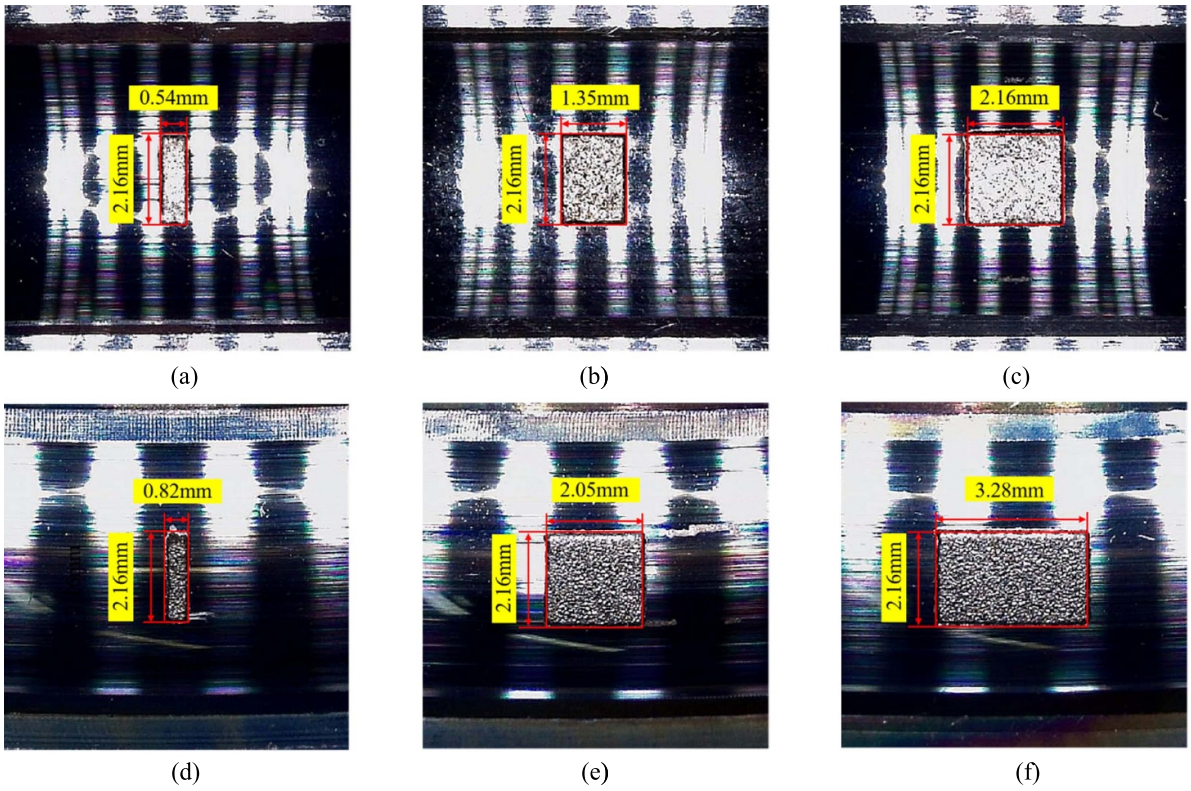

Figure 5. Photos of local defects of inner and outer raceways under different severity:(a) slight fault of inner raceway, (b) moderate fault of inner raceway, (c) severe fault of inner raceway, (d) slight fault of outer raceway, (e) moderate fault of outer raceway, (f) severe fault of outer raceway.

Table 1. Dataset description of case I.

Label	Speeds (rpm)	Types	Damage level
0	600 & 900 & 1200	Health	—
1	600 & 900 & 1200	Inner raceway fault	Slight
2	600 & 900 & 1200	Inner raceway fault	Moderate
3	600 & 900 & 1200	Inner raceway fault	Severe
4	600 & 900 & 1200	Outer raceway fault	Slight
5	600 & 900 & 1200	Outer raceway fault	Moderate
6	600 & 900 & 1200	Outer raceway fault	Severe

(c) Multi-source DA: All of these solutions of this part adopt multisource domain adaptation methods, and several common distance metrics are selected to replace the LMMD loss of MSDAN for comparison, including MMD loss and CORAL loss [42]. Meanwhile, the latest MSSA [43] transfer learning method is also introduced for comparison.

The training of all domain adaptation methods was implemented in the Pytorch framework. The initial learning rate of MSDAN was set differently according to the different adaptation tasks. The initial learning rates are described in table 3. It is further stated that lr[0] is the initial learning rate of the shared feature extractor, lr[1] is the initial learning rate of the private feature extractor and classifier, and the gradient descent strategy uses a SGD method with a momentum of 0.9. We set the number of iterations to 15 000 and the batch-size to 14. All results are the average diagnostic accuracy of five training runs. In addition, the trade-off parameters α and β determine the weight of LMMD loss and classifier difference loss in the total loss function. We change β from 0 to 1 to suppress noisy activations in the early stages of training, and it can be set to:

$$\beta = \frac{2}{1+\exp\left(-\theta\left(\frac{i}{I}\right)\right)} - 1 \tag{11}$$

where i indicates ith iteration in the training, I indicates the number of the iteration, and $\theta = 10$ is fixed throughout the experiments [44]. To ensure the accuracy of the classification, α should also be selected appropriately. We set $\alpha = \lambda\beta$. For λ, we assigned values at intervals of 0.1 over the range [0.1,1] and conducted an experimental study. We found that λ values set too low would result in LMMDs between domains having too little impact on the overall training of the model and that the transferable features of the source and target domains were maladaptive after training. In contrast, setting λ too high will lead to degradation of the source domain learning, i.e. the source domain model will be under-fitted, further affecting the recognition accuracy of the target domain.

Finally, we set $\lambda = 0.5$ to obtain better cross-domain diagnostic performance.

4.1.3. Experiment result and analysis. The diagnostic accuracies of the various methods under different domain adaptation tasks are shown in table 4 and figure 6. The significance of bold values in table 4 is the result with the highest diagnostic accuracy in this task. Among the three

Table 2. Three adaptation tasks of case I.

Adaptation task	Source domains	Target domain	Trained source samples	Trained target samples	Tested target samples
$R_1 + R_2 \rightarrow R_3$	600 rpm, 900 rpm	1200 rpm	$2 \times 7 \times 500$	7×500	7×500
$R_1 + R_3 \rightarrow R_2$	600 rpm, 1200 rpm	900 rpm	$2 \times 7 \times 500$	7×500	7×500
$R_2 + R_3 \rightarrow R_1$	900 rpm, 1200 rpm	600 rpm	$2 \times 7 \times 500$	7×500	7×500

Table 3. Hyperparameters setting based on MSDAN.

Adaptation task	$R_1 + R_2 \rightarrow R_3$	$R_1 + R_3 \rightarrow R_2$	$R_2 + R_3 \rightarrow R_1$
Batch-size	14	14	14
lr[0]	0.001	0.001	0.001
lr[1]	0.001	0.0015	0.002

groups of domain adaptation tasks, the diagnostic accuracy of the method proposed in this paper outperforms the other methods, with an average diagnostic accuracy of 99.63%. In the group of $R_1 + R_2 \rightarrow R_3$ domain adaptation tasks, the diagnostic accuracy even reached 100%. More specifically, by comparing the diagnostic accuracy of MSDAN and several popular intelligent fault diagnosis methods, the following conclusions are drawn.

(a) Baseline is not suitable for handling diagnostic tasks with cross-domain differences because its diagnostic accuracy is much lower than other methods due to lack of domain adaptation, which cannot learn the invariant features of each domain and reduce the differences between the source domain and target domain. Therefore, it is not suitable for handling diagnostic tasks with cross-domain differences, thus validating the effectiveness of domain adaptation in the cross-domain diagnosis of rolling bearing fault states.
(b) Whether the adaptation network is based on feature statistical moment matching or adversarial learning, its source-combine DA scheme outperforms single-best DA in terms of diagnostic performance. The reason is that the combination of multiple source domains gives us richer training data and can provide more valid diagnostic knowledge. It is further proof of the value of multisource data.
(c) Multi-source DA has a substantial performance improvement over source-combine DA. The reason is that source-combine DA is still essentially a solution to the problem of multisource domain adaptation using a single-source domain adaptation approach, which ignores the differences between individual source domains. Therefore, it is important to study the relationship between multiple source domains and the adaptation problem with the target domain.
(d) The diagnostic accuracy of the MSSA and MSDAN based on LMMD is greatly improved, especially our model improves the cross-domain diagnostic performance significantly by 4.05% and 4.52% compared to the multisource domain adaptation network based on CORAL loss and MMD loss, respectively. Next, the proposed model achieves better results than MSSA for all diagnostic tasks due to the fact that MSDAN minimizes the variance of each particular classifier and learns the generalized classification boundaries of the target samples better. In addition, MSDAN has the smallest standard deviation and better robustness, both for multiple diagnostic results of the same experiment and for different diagnostic tasks. The encouraging result demonstrates that MSDAN can align the distribution between the relevant subdomains by capturing the fine-grained information of each category, thus matching the distribution of features between multiple source domains and target domain more effectively. It also reflects the advantages of the method proposed in this paper in the current deep transfer fault diagnosis.

In order to intuitively understand the domain adaptation process, the t-distributed stochastic neighbor embedding (t-SNE) algorithm [45] is used to transform the extracted high-dimensional features into a two-dimensional feature vector and directly plot the distribution of the learned features. Furthermore, to give a more intuitive analysis, the cross-domain diagnostic task $R_1 + R_2 \rightarrow R_3$ is selected. The distribution of features learned by each model in the target domain through t-SNE visualization analysis are illustrated in figure 7. From figure 7(a), it can be seen that the Baseline model learns transferable features with severe distribution differences, poor clustering of target domain features and small inter-class distances. Therefore, when the model only trains samples in the source domain, it cannot effectively classify the unlabeled samples in the target domain. The results of the single-best DA and source-combine DA schemes in figures 7(b)–(f) show that the target domain is clustered into seven clusters corresponding to the seven health conditions of the target domain. However, there is still a large degree of overlap among data for some of the categories, which indicates that the domain adaptation results of the algorithm are not satisfactory after iterative convergence, and the extracted transferable features are not the optimal domain invariant features with the possibility of further improvement. As presented in figures 7(g)–(j), the same health conditions can be clustered well, especially the visualization result of our method is divided into seven well-defined clusters, further demonstrating its high performance and superiority.

4.2. Case II: fault diagnosis on variable machines

In this section, to further validate the effectiveness of our proposed method, we perform transfer diagnoses between

Table 4. Comparisons of the diagnostic accuracy (%) under different domain adaptation tasks.

Programs	Method	$R_1 + R_2 \rightarrow R_3$	$R_1 + R_3 \rightarrow R_2$	$R_2 + R_3 \rightarrow R_1$	Average
Single-best DA	Baseline	77.31 ± 1.775	72.74 ± 3.390	69.14 ± 2.973	73.06
	DDC	91.60 ± 0.884	85.60 ± 1.066	82.57 ± 2.305	86.59
	DAN	89.03 ± 1.859	87.74 ± 1.322	85.11 ± 1.646	87.29
	DANN	90.26 ± 2.437	87.20 ± 2.536	86.31 ± 3.088	87.92
Source-combine DA	DAN_{com}	91.66 ± 1.729	90.54 ± 1.453	85.26 ± 1.666	89.15
	$DANN_{com}$	92.71 ± 2.128	87.91 ± 1.813	87.34 ± 2.259	89.32
Multi-source DA	$MSDAN_{coral}$	97.17 ± 2.758	96.80 ± 1.889	92.77 ± 1.128	95.58
	$MSDAN_{mmd}$	96.03 ± 0.650	95.60 ± 0.839	93.71 ± 1.211	95.11
	MSSA	99.96 ± 0.046	98.66 ± 0.706	98.75 ± 0.892	99.12
	MSDAN	**100.00 ± 0.000**	**99.83 ± 0.116**	**99.06 ± 0.230**	**99.63**

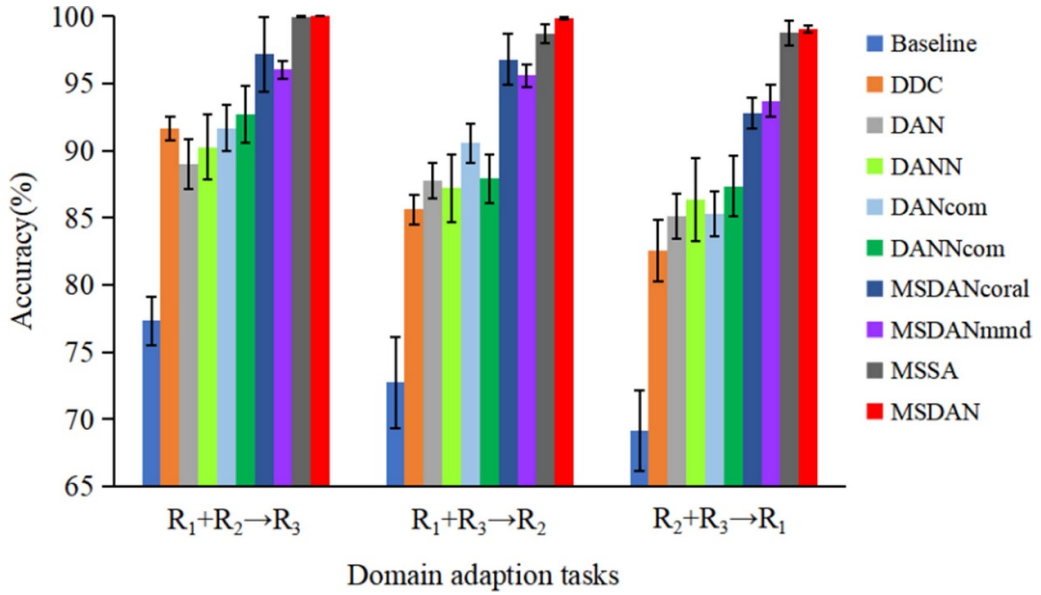

Figure 6. The average accuracy of case I.

different machines. With varying measurement environments, diverse environments and different machine architectures between separate machines, there is more variability between domains in this type of transfer diagnosis task, and the cross-domain diagnosis is more challenging. This section conducts multisource domain adaptation experiments based on self-collection datasets, including SpectraQuest MFS dataset (I) and self-built test rig dataset (II) and open-source datasets, including MFPT dataset (III) and PU dataset (IV), respectively. By comparing the experimental results of the current classical deep transfer learning methods, the superiority of MSDAN is verified.

4.2.1. Dataset description. The SpectraQuest MFS dataset (I) was collected by the test rig in section 4.1.1. The dataset contains three health conditions: healthy (N), inner ring fault (IRF) and outer ring fault (ORF). Here, the IRF level is moderate and the ORF level is slight. Each health condition data files with different operating conditions (driving speeds: 600 rpm/900 rpm/1200 rpm and vertical radial load: 49 N) are used to generate data samples. Also, the same health condition under different operation conditions is considered to be in the same category.

The Self-built test rig dataset (II) was collected by the test rig shown in figure 8(a). Compared to the SpectraQuest MFS test rig, this test rig utilizes an electric cylinder loading method and uses a higher motor power as well as a sampling frequency of 51.2 kHz. The dataset contains three folders corresponding to the three health conditions (N, IRF, ORF). In this experiment, the fault sizes are all different from the SpectraQuest MFS dataset, with the IRF level being slight and the ORF level being server. The same health condition under different operation conditions (driving speeds: 600 rpm/900 rpm/1200 rpm and horizontal radial load: 1200 N) is treated as one category.

The machinery failure prevention technology (MFPT) dataset (III) is a dataset of faulty bearings collected by the Mechanical Failure Society and contains normal (N) vibration data, IRF vibration data under various loads and ORF vibration data under various loads. In this experiment, the test rig runs at 1500 rpm. Furthermore, the normal dataset is sampled at

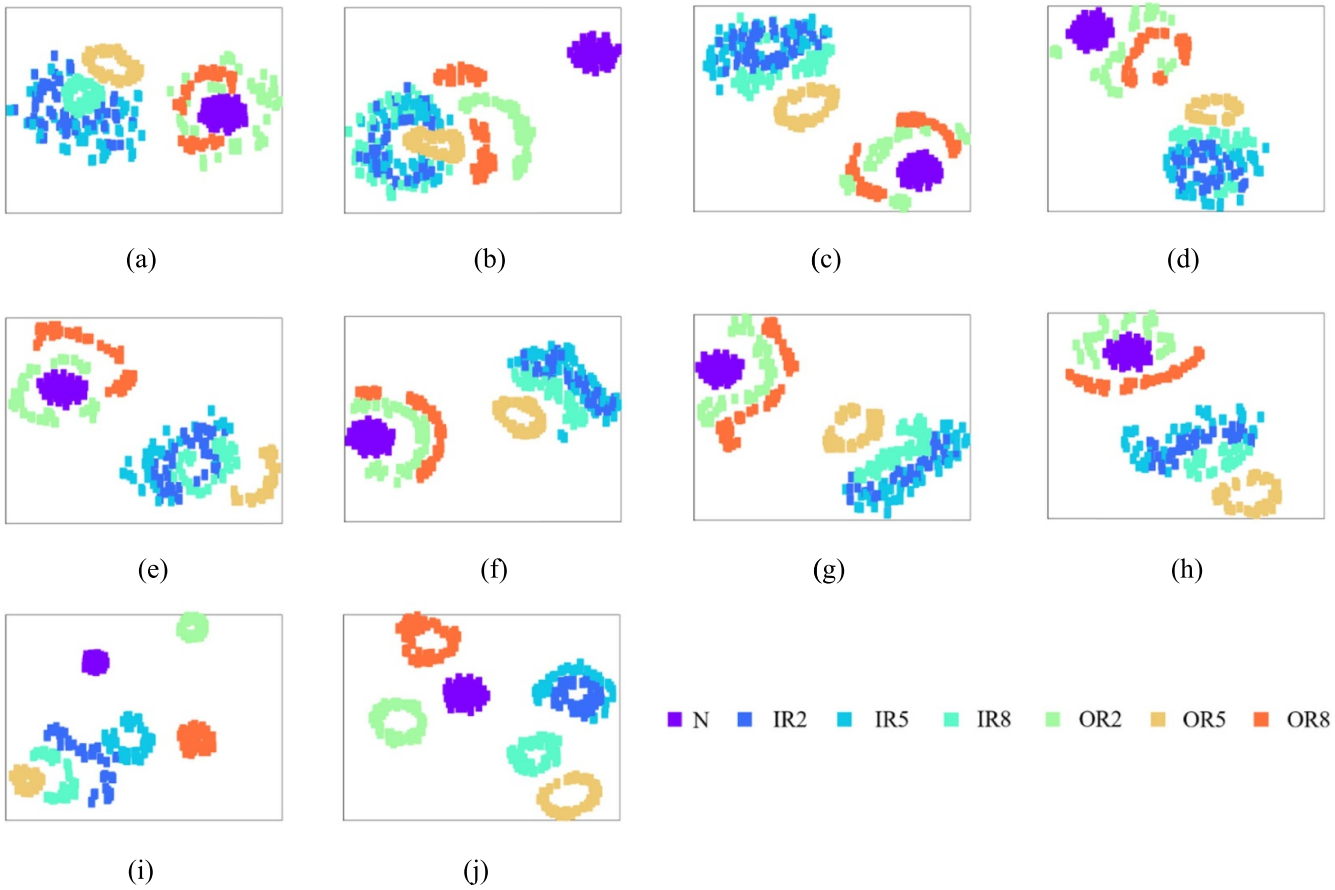

Figure 7. Visualizations of different domain adaptation methods in case I: (a) baseline, (b) DDC, (c) DAN, (d) DANN, (e) DAN_{com}, (f) $DANN_{com}$, (g) $MFSAN_{coral}$, (h) $MFSAN_{mmd}$, (i) MSSA and (j) MSDAN.

(a)

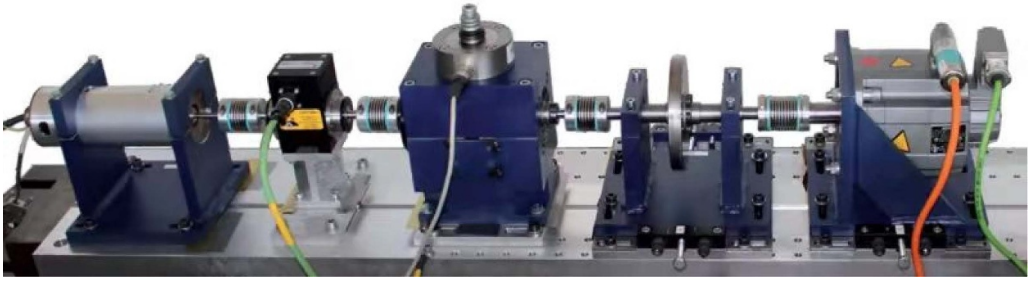

(b)

Figure 8. Photos of test rigs: (a) self-built test rig and (b) PU.

Table 5. Three adaptation tasks of case II.

Adaption task	Trained source samples	Trained target samples	Tested target samples
I + II + III → IV	3 × 3 × 400	3 × 400	3 × 400
I + II + IV → III	3 × 3 × 400	3 × 400	3 × 400
I + III + IV → II	3 × 3 × 400	3 × 400	3 × 400
II + III + IV → I	3 × 3 × 400	3 × 400	3 × 400

Table 6. Comparisons of the diagnostic accuracy (%) under different adaption tasks.

Programs	Methods	I + II + III → IV	I + II + IV → III	I + III + IV → II	II + III + IV → I	Avg
Single-best DA	Baseline	64.67 ± 4.494	58.83 ± 3.775	73.33 ± 4.381	66.17 ± 4.703	65.75
	DDC	86.67 ± 3.502	83.33 ± 1.180	89.50 ± 1.644	94.83 ± 3.221	88.58
	DAN	88.42 ± 2.636	84.42 ± 1.322	95.50 ± 2.127	98.75 ± 0.917	91.77
	DANN	90.83 ± 1.553	85.50 ± 1.394	94.67 ± 2.941	97.08 ± 2.407	92.02
Source-combine DA	DAN_{com}	91.33 ± 2.712	85.25 ± 1.424	94.08 ± 1.147	95.17 ± 2.565	91.46
	$DANN_{com}$	93.16 ± 0.908	87.16 ± 1.725	92.42 ± 1.218	96.33 ± 1.903	92.27
Multi-source DA	$MSDAN_{coral}$	92.83 ± 1.063	85.67 ± 0.080	94.58 ± 0.945	97.33 ± 1.655	92.60
	$MSDAN_{mmd}$	94.58 ± 0.826	86.25 ± 1.447	96.17 ± 1.107	95.50 ± 1.119	93.13
	MSSA	**95.12 ± 0.765**	87.04 ± 1.121	97.64 ± 0.627	99.48 ± 0.322	94.82
	MSDAN	93.42 ± 0.770	**87.67 ± 0.396**	**98.75 ± 0.535**	**99.83 ± 0.155**	**94.92**

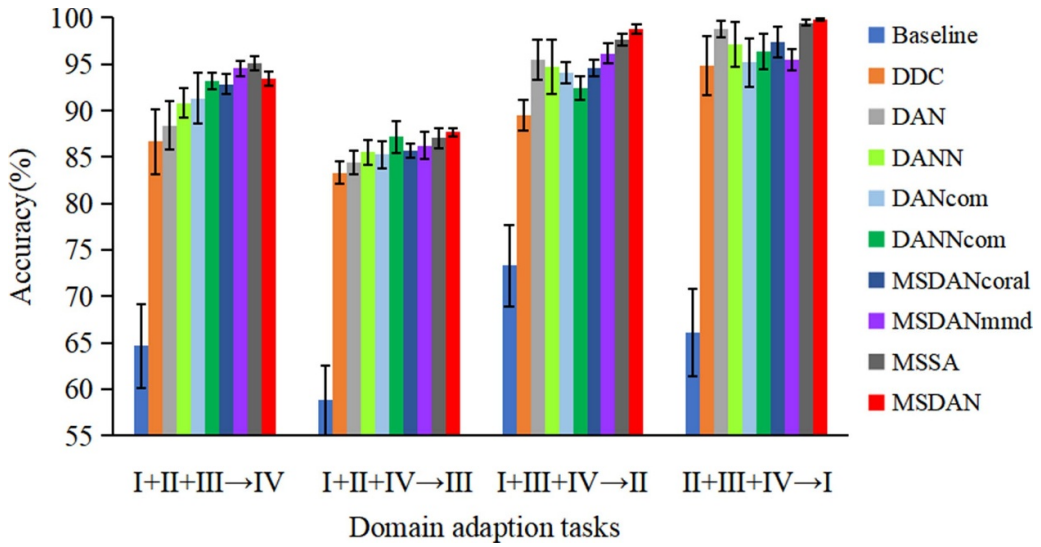

Figure 9. The average accuracy of case II.

97.656 kHz with a load condition of 270 lbs. The IRF dataset is sampled at 48.828 KHz with load conditions of 0, 50 and 100 lbs. And the ORF dataset is sampled at 48.828 KHz a with load conditions of 25, 50 and 100 lbs. The same health condition under different operation conditions is considered to be in the same category.

The Paderborn University (PU) dataset (IV) was collected by the University of Paderborn by the test rig shown in figure 8(b) and contained three types of faults: normal condition (N) and two artificial damage faults (IRF, ORF). The experimental object is the rolling bearing of type 6203. The test rig runs at 1500 rpm. Also, the same health condition under different operation conditions (driving speeds: 1500 rpm, radial load: 1000 N and load torque: 0.7 Nm/0.1 Nm) is treated as one category.

Each health condition of the above dataset contains 400 samples with a length of 8192 under varying operating conditions. In this case, we construct four multisource domain adaptation tasks as shown in table 5. Each domain adaptation task is trained jointly by three source labeled domains and an unlabeled target domain. The comparison method and implementation details are consistent with section 4.1.2.

4.2.2. Experiment result and analysis. Table 6 and figure 9 list the experimental results of four rolling bearing diagnosis

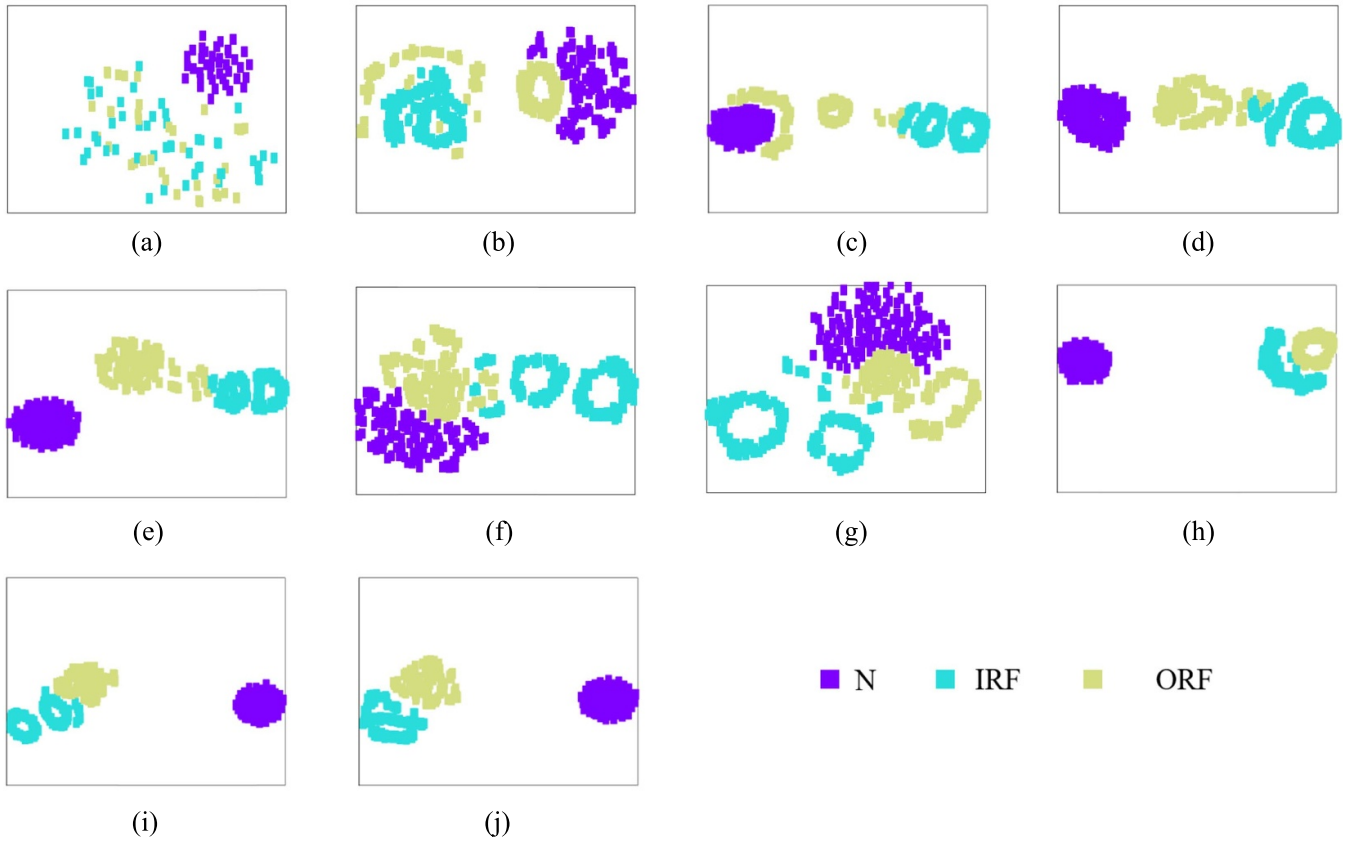

Figure 10. Visualizations of different domain adaptation methods in case II: (a) baseline, (b) DDC, (c) DAN, (d) DANN, (e) DAN_{com}, (f) $DANN_{com}$, (g) $MFSAN_{coral}$, (h) $MFSAN_{mmd}$, (i) MSSA and (j) MSDAN.

tasks. It can be seen that the method proposed in this paper achieves the highest diagnostic accuracy among the four multisource domain adaptation diagnosis tasks compared to multiple intelligent fault diagnosis methods. Moreover, we have drawn the following conclusions.

(a) The average accuracy of the intelligent fault diagnosis method based on deep learning without domain adaptation is 65.75%, which is much lower than that of other domain adaptation intelligent fault diagnosis methods, indicating that both robustness and generalization are poor when deep learning is applied to cross-domain diagnosis tasks with distributional differences.

(b) In the single-source domain adaptation, the tasks I + III + IV → II and II + III + IV → I are more effective compared to the tasks I + II + III → IV and I + II + IV → III. It is because the SpectraQuest MFS dataset (I) and the Self-built test rig dataset (II) were collected in different test rigs, but the operating speed conditions and bearing types were consistent, so there were fewer differences between the source domain and target domain, which facilitated the domain adaptation. In contrast, when both the test rig and the operating conditions differ significantly, this can lead to different vibration patterns of the bearings and large differences in the collected signals, which negatively affects the cross-domain diagnosis of the bearings.

(c) Simply combining multiple source domain data and using a single source domain adaptation algorithm directly on the combined data can improve the accuracy of cross-domain diagnosis to some extent. However, the diagnostic accuracy of the source-combine DA in tasks I + III + IV → II and II + III + IV → I is lower than that of its corresponding single-best DA. It is maybe because domain differences exist between different source domains, and the degree of similarity between different source domains and the target domain also varies. For example, in the I + III + IV → II domain adaptation task, the SpectraQuest MFS dataset (I) and the Self-built test rig dataset (II) are more similar, while the MFPT dataset (III) and the PU dataset (IV) are less similar to the Self-built test rig dataset (II), thus, simply combining I, III and IV is equivalent to increasing the difference between the combined source domains and target domain, which will lead to negative transfer phenomenon, illustrating the necessity of effectively combining multiple source domains for domain adaptation.

(d) Among the four domain adaptation tasks, the average diagnostic accuracy of MSDAN is 94.92%, which is significantly better than other diagnostic methods. It suggests that MSDAN can more rationally utilize the feature information of each source domain and perform a more refined alignment to provide better diagnostic performance, which attenuates the effect of negative transfer. However, MSSA

obtained better results on the I + II + III → IV task, which may be due to the fact that MSSA performed an inconsistent weighted average of the predictions of all classifiers, increasing reliability in terms of target prediction. From those results, it can be seen that our model outperformed MSSA for the remaining three diagnostic tasks. It is due to the alignment of multiple classifiers by mean differences and by averaging predictions from different sources of classifiers, which further increases the consistency of predictions for target samples which are close to domain boundaries. In addition, although most of the methods achieve an average accuracy of over 90%, they have large fluctuations across multiple experiments on the same task or between tasks. The experimental results show that MSDAN has better generalization and robustness across transfer diagnosis tasks, promising more complex fault diagnosis.

We randomly select the cross-domain diagnostic task I + III + IV → II and use the t-SNE algorithm for feature visualization to obtain the results as shown in figure 10. Compared with other intelligent fault diagnosis models, we can see that the visualization results of MSDAN show clear boundaries for each category and a consistent data distribution between the source domain and target domain, confirming that the subdomain alignment we used can not only align well globally, but also align the distribution of subdomains of the same category with more terrific refinement. In summary, the proposed method is more useful for learning common features of multiple data domains, and their cross-domain adaptation capabilities are stronger.

5. Conclusions

To achieve more accurate and reliable fault diagnosis of rolling bearing under the data distribution shift, this paper proposes a MSDAN. First, the raw vibration signal is directly input into the network and generic features are extracted using a shared feature extractor. Then, domain-exclusive private feature extractors are used to map multiple source domains and the target domain data with different distributions to multiple different feature spaces. Finally, we propose a two-stage alignment scheme. The first one is to construct subdomains through the relationship between categories and introduce LMMD to reduce the distribution differences between domains, and the second is to align the output of the classifier with the target samples through the mean difference. Benefiting from three aspects (a) using the raw vibration signal of the bearing as input, the end-to-end diagnosis from data to identification is achieved, avoiding human interference, (b) collecting data from multiple source domains to match the target domain, enabling the target domain to learn more comprehensive feature information, and (c) effectively aligning the distribution of subdomains of the same category, solving the existing methods that only using global alignment and ignoring the fine-grained information of the category which leads to degradation of diagnostic accuracy. In two bearing fault diagnosis cases, including cross-operating-condition and cross-machine, eight popular domain adaptation methods for fault diagnosis are selected for comparison. The experimental results show that the proposed method has good robustness and achieves the best diagnostic results during the multisource domain adaptation process, validating the superiority of MSDAN. Therefore, the proposed method provides a promising tool for solving the problem of cross-domain fault diagnosis in real industrial scenarios.

In addition, the issue of data quality in multiple source domains is worth considering due to the interference of the working environment during data acquisition. Sample optimization may be researched to further boost fault diagnosis accuracy.

Data availability statement

The data that support the findings of this study are openly available at the following URL: https://github.com/hitwzc/Bearing-datasets.

Acknowledgments

The research was supported by the National Natural Science Foundation of PR China (No. 51975143) and the Fundamental Research Funds for the Central Universities of China (HIT.NSRIF.201638).

ORCID iD

Zhichao Wang https://orcid.org/0000-0003-4802-8187

References

[1] Yang B, Lei Y, Jia F and Xing S 2018 An intelligent fault diagnosis approach based on transfer learning from laboratory bearings to locomotive bearings *Mech. Syst. Signal Process.* **122** 692–706
[2] Liu R, Yang B, Zio E and Chen X 2018 Artificial intelligence for fault diagnosis of rotating machinery: a review *Mech. Syst. Signal Process.* **108** 33–47
[3] Zhao M and Zuo M 2018 A new strategy for rotating machinery fault diagnosis under varying speed conditions based on deep neural networks and order tracking *ICMLA* (https://doi.org/10.1109/ICPHM.2018.8449003)
[4] Wang W, Li Y and Song Y 2022 Fault diagnosis method of vehicle engine via HOSVD-HOALS hybrid algorithm-based multi-dimensional feature extraction *Appl. Soft Comput.* **166** 108293
[5] Lecun Y, Bengio Y and Hinton G 2015 Deep learning *Nature* **521** 436–44
[6] Rui Z, Yan R, Chen Z, Mao K and Gao R 2019 Deep learning and its applications to machine health monitoring *Mech. Syst. Signal Process.* **115** 213–37
[7] Zhao K, Jiang H, Li X and Wang R 2019 An optimal deep sparse autoencoder with gated recurrent unit for rolling bearing fault diagnosis *Meas. Sci. Technol.* **31** 015005
[8] He M and He D 2017 Deep learning based approach for bearing fault diagnosis *IEEE Trans. Ind. Appl.* **53** 3057–65

[9] Khan S and Yairi T 2018 A review on the application of deep learning in system health management *Mech. Syst. Signal Process.* **107** 241–65

[10] Eren L, Ince T and Kiranyaz S 2019 A generic intelligent bearing fault diagnosis system using compact adaptive 1D CNN classifier *J. Signal Process. Syst. Signal Image Video Technol.* **91** 179–89

[11] Lei Y, Yang B, Jiang X, Jia F and Nandi A 2020 Applications of machine learning to machine fault diagnosis: a review and roadmap *Mech. Syst. Signal Process.* **138** 106587

[12] Zhang L, Lin J, Liu B, Zhang Z, Yan X and Wei M 2019 A review on deep learning applications in prognostics and health management *IEEE Access* **7** 162415–38

[13] Zhang R, Tao H, Wu L and Guan Y 2017 Transfer learning with neural networks for bearing fault diagnosis in changing working conditions *IEEE Access* **5** 14347–57

[14] Pan S and Qiang Y 2010 A survey on transfer learning *IEEE Trans. Knowl. Data Eng.* **22** 1345–59

[15] An J, Ai P and Liu D 2020 Deep domain adaptation model for bearing fault diagnosis with domain alignment and discriminative feature learning *Shock Vib.* **2020** 1–14

[16] Chen C, Fu Z, Chen Z, Cheng Z and Jin X 2021 Towards self-similarity consistency and feature discrimination for unsupervised domain adaptation *Signal Process. Image Commun.* **94** 116232

[17] Long M, Wang J, Cao Y, Sun J and Yu P 2016 Deep learning of transferable representation for scalable domain adaptation *IEEE Trans. Knowl. Data Eng.* **28** 2027–40

[18] Han T, Liu C, Yang W and Jiang D 2018 Deep transfer network with joint distribution adaptation: a new intelligent fault diagnosis framework for industry application *ISA Trans.* **97** 269–81

[19] Zhang B, Li W, Li X and See-Kiong N 2019 Intelligent fault diagnosis under varying working conditions based on domain adaptive convolutional neural networks *IEEE Access* **6** 66367–84

[20] Qian C, Shen Y and Huo C 2022 An intelligent fault diagnosis method for rolling bearings based on feature transfer with improved DenseNet and joint distribution adaptation *Meas. Sci. Technol.* **33** 025101

[21] Wu Z, Jiang H, Zhao K and Li X 2019 An adaptive deep transfer learning method for bearing fault diagnosis *Measurement* **151** 107227

[22] Borgwardt K, Gretton A, Rasch M, Kriegel H, Schlkopf B and Smola A 2006 Integrating structured biological data by kernel maximum mean discrepancy *Bioinformatics* **22** e49–57

[23] Gretton A, Borgwardt K, Rasch M, Scholkopf B and Smola A 2012 A kernel two-sample test *J. Mach. Learn. Res.* **13** 723–73

[24] She D, Peng N, Jia M and Pecht M 2020 Wasserstein distance based deep multi-feature adversarial transfer diagnosis approach under variable working conditions *J. Instrum.* **15** P06002

[25] Ganin Y, Ustinova E, Ajakan H, Germain P, Larochelle H and Laviolette F 2015 Domain-adversarial training of neural networks (arXiv:1505.07818 [stat.ML])

[26] Zhao J and Huang W 2022 Transfer learning method for rolling bearing fault diagnosis under different working conditions based on CycleGan *Meas. Sci. Technol.* **33** 025003

[27] Zhang W, Li X, Ma H, Luo Z and Li X 2021 Universal domain adaptation in fault diagnostics with hybrid weighted deep adversarial learning *IEEE Trans. Ind. Inform.* **17** 7957–67

[28] Wang Y, Sun X, Li J and Yang Y 2021 Intelligent fault diagnosis with deep adversarial domain adaptation *IEEE Trans. Instrum. Meas.* **70** 2503509

[29] Chen Z, He G, Li J, Liao Y and Li W 2020 Domain adversarial transfer network for cross-domain fault diagnosis of rotary machinery *IEEE Trans. Instrum. Meas.* **69** 8702–12

[30] Xu D, Li Y, Song Y, Jia L and Liu Y 2021 IFDS: an intelligent fault diagnosis system with multisource unsupervised domain adaptation for different working conditions *IEEE Trans. Instrum. Meas.* **70** 3526510

[31] Shi Y, Deng A, Ding X, Zhang S and Li J 2022 Multisource domain factorization network for cross-domain fault diagnosis of rotating machinery: an unsupervised multisource domain adaptation method *Mech. Syst. Signal Process.* **164** 108219

[32] Zheng H, Wang R, Yang Y, Li Y and Xu M 2019 Intelligent fault identification based on multisource domain generalization towards actual diagnosis scenario *IEEE Trans. Ind. Electron.* **67** 1293–304

[33] Zhang Y, Ren Z, Zhou S and Yu T 2020 Adversarial domain adaptation with classifier alignment for cross-domain intelligent fault diagnosis of multiple source domains *Meas. Sci. Technol.* **32** 035102

[34] Wei D, Han T, Chu F and Zuo M 2021 Weighted domain adaptation networks for machinery fault diagnosis *Mech. Syst. Signal Process.* **158** 107744

[35] Yang S, Kong X, Wang Q, Li Z, Cheng H and Yu L 2021 A multi-source ensemble domain adaptation method for rotary machine fault diagnosis *Measurement* **186** 110213

[36] Kumar A, Sattigeri P, Wadhawan K, Karlinsky L, Feris R, Freeman W and Wornell G 2018 Co-regularized alignment for unsupervised domain adaptation *Adv. Neural Inf. Process. Syst.* **2018** 9367–78

[37] Zhu Y, Zhuang F, Wang J, Ke G, Chen J, Bian J and He Q 2020 Deep subdomain adaptation network for image classification *IEEE Trans. Neural Netw. Learn. Syst.* **32** 1713–22

[38] Smola A, Gretton A, Song L and Scholkopf B A 2007 Hilbert space embedding for distributions *Int. Conf. on Algorithmic Learning Theory* vol 4754 pp 13–31

[39] Tzeng E, Hoffman J, Zhang N, Saenko K and Darrell T 2014 Deep domain confusion: maximizing for domain invariance (arXiv:1412.3474 [cs.CV])

[40] Long M *et al* 2015 Learning transferable features with deep adaptation networks *Proc. 32nd Int. Conf. on Machine Learning* vol 37 pp 97–105

[41] Ganin Y *et al* 2016 Domain-adversarial training of neural networks *J. Mach. Learn. Res.* **17** 2096–2030

[42] Chen R and Ren G 2020 Correlation alignment with attention mechanism for unsupervised domain adaptation *Web Intellifence* **18** 261–7

[43] Tian J, Han D, Li M and Shi P 2022 A multi-source information transfer learning method with subdomain adaptation for cross-domain fault diagnosis *Knowl.-Based Syst.* **243** 108446

[44] Ganin Y and Lempitsky V 2015 Unsupervised domain adaptation by backpropagation (arXiv:1409.7495v2 [stat.ML])

[45] Van D and Hinton G 2008 Visualizing data using t-SNE *J. Mach. Learn. Res.* **9** 2579–605